Photodiagnosis and Photodynamic Therapy 28 (2019) 300–307

Contents lists available at ScienceDirect

Photodiagnosis and Photodynamic Therapy

journal homepage: www.elsevier.com/locate/pdpdt

Enhanced melanoma cell-killing by combined phototherapy/radiotherapy using a mesoporous platinum nanostructure

F. Salehi[a,b], F. Daneshvar[a,b], M. Karimi[b], R. Dehdari Vais[b], M.A. Mosleh-Shirazi[c], N. Sattarahmady[a,b,*]

[a] Department of Medical Physics, School of Medicine, Shiraz University of Medical Sciences, Shiraz, Iran
[b] Nanomedicine and Nanobiology Research Center, Shiraz University of Medical Sciences, Shiraz, Iran
[c] Physics Unit, Department of Radio-Oncology, Shiraz University of Medical Sciences, Shiraz, Iran

ARTICLE INFO

Keywords:
Pt
Mesopore structure
Laser therapy
Radiation therapy
Cell viability
Reactive Oxygen species

ABSTRACT

Background: Metal nanomaterials have a significant potential as photosensitizer and radiosensitizer. The purpose of this study was to evaluate the cytotoxicity of a platinum mesoporous nanostructure (Pt MN) toward a melanoma cancer cell line upon combined laser radiation (808 nm, 1 and 1.5 W cm^{-2}) and X-ray irradiation (6 MV, 2, 4, and 6 Gy).

Methods: Pt MN was synthesized by a simple procedure and characterized by field emission scanning and transmission electron microscopy. A mouse malignant melanoma cell line C540 (B16/F10) was treated with Pt MN, laser light and/or X-ray.

Results: Pt MN had a mesoporous structure with a sponge-resemble shape comprised of ensembles of very small adhered particles of < 11 nm and about 5-nm pores. While Pt MN represented a low toxicity toward and considerable uptake into the cell line in a concentration range of 10–100 μg mL^{-1}, laser light radiation alone was also not toxic, and X-ray irradiation alone induced a limited toxicity, Pt MN was toxic against the cells in a dose dependent manner upon laser light radiation, X-ray irradiation, or their combined exposure. The killing efficacy of Pt MN upon X-ray irradiation was more obvious at 72 h post-treatment. The combined exposure (laser radiation followed by X-ray irradiation) led to a deep cell killing and a very low melanoma cell viability (~1%). Significant melanoma cancer cell killing of Pt MN was due to reactive oxygen species (ROS) production upon combined exposure of laser and X-ray, while cell killing upon laser light radiation was due to heat generation.

Conclusion: Pt MN was introduced as a supreme laser/X-ray sensitizer for treatment of cancer with a high ability to produce ROS and a potent impact on decreasing cell viability.

1. Introduction

Since conventional strategies of cancer treatment can generate serious adverse effects, discovery of less toxic but still successful novel strategies for cancer treatment is a significant aim for medical researchers [1]. Nanotechnology has resulted in outstanding results that suggest a potential for nanomaterial applications in therapeutic and diagnostic strategies [2–5]. Also, the design of new nanomaterials effectively applicable for both treatments and diagnosis is a priority [6]. Phototherapy approaches including photothermal therapy (PTT) and photodynamic therapy (PDT) for tumor suppression have been successful in the treatment of tumors. In PTT, phototransducer nanomaterials induce energy conversion of near-infrared (NIR) light to heat, and thermal enhancement results in the tumor cell annihilation [7]. In PDT, radiation of a visible light in combination with a photosensitizer and oxygen molecule/oxygen-containing species produces reactive oxygen species (ROS) that induce vascular and cellular damages followed by cell death [8]. Due to limited penetration depth of visible light into tissues during PDT, PTT by NIR light, micro-induced PDT (MIPDT) by microwaves, sonodynamic therapy (SDT) by ultrasound, and X-ray-induced PDT (X-PDT) are proposed as alternatives [9]. During the last route (i.e. X-PDT), radiation therapy (RT) that generates different ROS upon radiolysis of water is accelerated using a nanomaterial. Nanomaterials are excitable by the X-ray source of RT, and further generate ROS. The main advantage of X-PDT is that X-ray (generally with energy ranging from 50 kV to 6 MV and specially 6 MV employed for X-PDT)

* Corresponding author at: Department of Medical Physics, School of Medicine, Nanomedicine and Nanobiology Research Center, Shiraz University of Medical Sciences, Shiraz, Iran.
E-mail addresses: sattarahmady@yahoo.com, nsattar@sums.ac.ir (N. Sattarahmady).

https://doi.org/10.1016/j.pdpdt.2019.10.001
Received 31 May 2019; Received in revised form 1 September 2019; Accepted 4 October 2019
Available online 10 October 2019
1572-1000/

can penetrate deep inside the tissues up to 40 cm [9].

Synthesis and application of multi-purpose nanomaterials for medical goals are highly of interest and in progress. Examples include phototransducer nanomaterials for pressure wave induction and imaging (by photoacoustic instruments) [10], combined MR imaging and therapy [11], combined computed tomography (CT) imaging and therapy [12], contrast agents for combined CT and MR imaging [13], and nanomaterials of high atomic numbers (with high X-ray attenuation coefficients) for combined PTT and X-PDT (PTT/X-PDT) and 3D CT imaging [14,15]. Among the nanomaterials, mesoporous structures represent a high surface area and (re)activity arising from bicontinuous skeletons at the nanoscale, presence of interconnected hollow channels and mesopores, and structural thermostability [16–22]. Mesoporous platinum nanostructures stand for high (electro)catalytic activity, high loading capacity, easy functionalization, distinct electrical conductivity, and have acted as a nanocarrier for DNA and doxorubicine [23–25]. However, there is no approach regarding application of mesoporous structures in PTT, X-PDT or PTT/X-PDT. Also there is no report on the platinum mesoporous nanostructure (Pt MN) representing PTT, X-PDT or PTT/X-PDT properties.

In conventional RT, megavoltage X-ray irradiation beam from a linear accelerator is directed toward biological tissues, and leads to ionization of water or biological targets, damages to DNA (through direct or indirect processes), production of ROS, and finally tumor necrosis [26]. Serious limitations such as resistance of cancer cells to ionizing radiation, tumor recurrence, unwanted side effects and damages to healthy tissues in RT enforce the scientists to explore new approaches for improvement of the efficacy of RT [27,38]. Also, high-energy X-ray or γ-ray during RT induces destruction of both healthy and cancer cells. Repairing mechanisms of DNA break in cancer cells and existing hypoxic conditions (low-O_2 concentrations) are other limitations of RT efficacy [29,30]. At hypoxic conditions, the produced ROS by RT have minimum efficacy resulting in the repair of broken DNA (already induced by RT) and protection mechanisms to be proceeded [31].

As to enhancement of the selectivity and specificity of RT treatment, it is desired to reduce radiation dose and increase the X-ray deposition in the tumor area using radiosensitizers with strong X-ray attenuations [32]. High atomic number elements such as Au, Hf, Bi, Mo, Ta, rare earth elements and tantalum oxide as radiosensitizers enhance the X-PDT efficacy by supreme X-ray absorption [33,34]. Additionally, X-ray and γ-ray exposure to these high-Z elements intensify the production of photoelectrons, Compton electrons, Auger electrons, and secondary charged particles [35]. These phenomena result in more ionization and radical generations through direct and/or indirect processes, damages into cellular targets and DNA, and activation of the MAPKs and p53 pathways of cell apoptosis. Therefore, higher efficacy of X-PDT is attainable by concentrated doses in the target area [36]. In this way, the results of a Monte Carlo study indicated that a small amount of gold nanoparticles (NPs) led to significant increment in radiation absorption through two different mechanisms depending on the photon energy [37]. In kV range, X-ray induced production of Auger electrons through a photoelectric effect. These Auger electrons released all of their energy in the local site and induced serious biological effects. However and in spite of high mass energy absorption coefficients of gold NPs (compared to water) in the kV energy range, penetration depth was low [35,37]. On the other hand, in the radiotherapy photon energy range (6–20 MV), X-ray interacted with gold NPs through the Compton effect [37]. In spite of low mass energy absorption coefficients of gold NPs (compared to water) in MV energy range of radiation, higher efficacy was attained [35,37,38]. As for the utility of platinum materials, it should be mentioned that locating of high-Z elements in the track of incident ionizing particles (including photons) amplify ionization density as well as dose deposition due to increment of ionization cross section [39]. Incident ionizing particles and the produced secondary electrons excite electrons located in the inner and outer shells of these metals. The excited inner shell electrons produce Auger electrons, e.g., about ten Auger electrons are emitted upon ionization of platinum L-shell. Ultimately, water ionization and radical generation occur those induce DNA double and single strands break. All of the processes are accelerated using nanostructured high-Z elements [40].

Zhou et al. used polyglutamic acid nanogels loaded with polypyrrole as a sensitizer of X-PDT, PTT, or their combination both *in vitro* and *in vivo* for treatment of cancerous cells and tumor xenografts. Their results showed that the sequence of application of laser radiation and X-ray irradiation was important in the treatment efficacy. The results also indicated a concentration-dependent toxicity with an efficacy order of PTT/X-PDT > X-PDT/PTT > X-PDT, i.e. PTT followed by X-PDT (PTT/X-PDT) had more efficiency than the vice versa route (X-PDT followed by PTT, X-PDT/PTT) at the same sensitizer concentration [41]. In these studies, combination of PTT and X-PDT using a nanosensitizer provided advantages of both treatments: PTT improved blood flow and oxygen status of the tumor area to overcome hypoxia, and increase the cell absorption of X-ray [31,42]. Therefore, discovery of new nanosensitizers that enhance the efficacy of different therapeutic modalities is a promising strategy to improve treatment via synergistic or additive effects. In this regard, nanoscale metals are supreme candidates as dual sensitizers for NIR light and X-ray [43], and Pt nanomaterials are good candidates for X-PDT with a low toxicity [44].

In this study, a Pt MN was synthesized for PTT, X-PDT and PTT/X-PDT applications in mouse malignant melanoma cell line (C540 (B16/F10)) by a continuous-wave diode laser of 808-nm as a light source and a linear accelerator as an X-ray source. The physicochemical characterization of Pt MN and cell viability were evaluated.

2. Materials and methods

2.1. Materials

H_2PtCl_6, formic acid, Triton X-100, Tris-HCl, sodium dodecyl sulfate, NaCl and phosphate buffer salts were prepared from Merck (Germany). 2′,7′-dichlorodihydrofluorescein diacetate (DCHF-DA) and 3-(4,5-dimethylthiazol-2-yl)-2,5-diphenyl-tetrazolium bromide (MTT) were purchased from Sigma (USA), and dimethyl sulfoxide (DMSO) was prepared from Scharlau Chemie (Spain). The chemicals were used without further purification. Deionized (DI) water was used throughout the experiments.

2.2. Synthesis and characterization of Pt MN

For synthesis, 15 mL aqueous solution containing 1 mmol L^{-1} H_2PtCl_6, 1.75 mol L^{-1} formic acid and 10 mmol L^{-1} sodium dodecyl sulfate was prepared in a Teflon baker. The solution was continuously stirred at 500 rpm during the reaction at 40 °C for 3 h. The resultant Pt MN was centrifuged, washed several times with DI water, and dried at room temperature.

For characterization, filed-emission scanning electron microscopy (FESEM) was employed, and the corresponding images were recorded by a TESCAN Mira 3-XMU 116 microscope (Czech Republic). Transmission electron microscopy (TEM) was also employed, and TEM images were recorded by a Philips CM30 microscope (Germany).

UV-vis spectra were recorded using a Rayleigh UV2601 double beam spectrophotometer (China).

2.3. Light setups

Laser light was irradiated at 808 nm by a diode laser of Thorlabs (USA) with an optical output power of 1000 mW equipped with a benchtop temperature controller. Output laser power density was selected at 1.0 or 1.5 W cm^{-2} by changing the spot size of the output mounting lens and the distance between the lens and target. Laser light radiation time was 10 min.

The X-ray was produced by a 6 MV Elekta Compact medical linear

accelerator (Crawley, UK) delivering radiation doses of 2, 4 and 6 Gy at a dose rate of approximately 200 cGy min^{-1}. The cells in culture plates were placed at 100 cm distance from the source in a phantom consisting of 1 cm buildup and 5 cm backscatter Lucite sheets. A radiation field size of 20 × 20 cm^2 was used. Irradiation times to deliver 2, 4, and 6 Gy were approximately one, two and three minutes, respectively.

2.4. Cell line preparation

Mouse malignant melanoma cell line C540 (B16/F10) was purchased from Pasteur Institute (Iran). The cells were cultured in Roswell Park Memorial Institute-1640 (RPMI) from Gibco (USA) medium with 10% fetal bovine serum from Gibco (USA) and 1% antibiotic (penicillin-streptomycin) from Gibco (USA) at 37 °C in a humidified atmosphere of cell incubator containing 5% CO_2.

2.5. Pt MN effect on the cell viability upon laser radiation (PTT)

Temperature increment of the C540 (B16/F10) cell medium was measured with a thermoprobe of Lutron (Taiwan) with a 0.01 °C accuracy. The cells (1.0×10^4 cell $well^{-1}$) in 96-well plates were incubated with Pt MN (100 μg mL^{-1}), and the temperature was measured before and after laser radiation at a power density of 1.0 or 1.5 W cm^{-2} for 10 min.

C540 (B16/F10) cells at a density of 1.0×10^4 cell $well^{-1}$ were seeded into 96-well plates for 24 h to cell adhesion. The wells were divided into the following groups and incubated at 37 °C in a 5% CO_2 atmosphere.

- Control: Untreated cells (neither laser radiation nor Pt MN affection)
- N: Treated cells only with Pt MN at concentrations of 10, 50, and 100 μg mL^{-1}
- L1 and L1.5: Treated cells with laser radiation at power density of 1.0 (L1) or 1.5 W cm^{-2} (L1.5) for 10 min after 4 h
- NL1 and NL1.5: Treated cells firstly with Pt MN at concentrations of 10, 50, and 100 μg mL^{-1} for 4 h, followed by post treatment with laser radiation at power density of 1.0 (L1) or 1.5 W cm^{-2} (L1.5) for 10 min after 4 h

The incubation time for different groups of the cells was continued overnight at 37 °C and 5% CO_2, and then the cell viability was measured by the MTT assay. For this assay, the medium of the cells was substituted by 100 μL of 0.5 mg mL^{-1} MTT dissolved in phosphate buffer saline (PBS) and incubated at 37 °C for 4 h in dark. Then, the plates were centrifuged at 1800 rpm for 10 min and the culture supernatant was removed; then 100 μL of DMSO was added to dissolve the MTT formazan crystals. After centrifugation at 3500 rpm for 3 min, the supernatant was removed from each well and the optical density (OD) was recorded at 570 nm using a microplate reader of Biotek (USA). The cell viability was expressed as the ratio of the 570 nm absorbance of the treated and control cells.

2.6. Pt MN effect on cell viability upon X-ray irradiation (X-PDT)

C540 (B16/F10) cells at a density of 1.0×10^4 cell $well^{-1}$ were seeded into 96-well plates for 24 h to cell adhesion. The wells were divided into the following groups and incubated at 37 °C in a 5% CO_2 atmosphere.

- Control: Untreated cells (neither X-ray irradiation nor Pt MN affection)
- N: Treated cells only with Pt MN at concentrations of 10, 50, and 100 μg mL^{-1}
- X2, X4 and X6: Treated cells with X-ray irradiation at radiation doses of 2 (X2), 4 (X4) and 6 Gy (X6) after 4 h
- NX2, NX4 and NX6: Treated cells firstly with Pt MN at concentrations of 10, 50, and 100 μg mL^{-1} for 4 h, followed by post treatment with X-ray irradiation at radiation doses of 2 (NX2), 4 (NX4) and 6 Gy (NX6) after 4 h

The incubation time for different groups of the cells was continued overnight at 37 °C and 5% CO_2. Another similar set of experiments was also repeated with continuation of incubation time to 72 h for different groups. The cell viability was finally measured by the MTT assay.

2.7. Pt MN effect on cell viability upon PTT/X-PDT

C540 (B16/F10) cells at a density of 1.0×10^4 cell $well^{-1}$ were seeded into 96-well plates for 24 h to cell adhesion. The wells were divided into the following groups and incubated at 37 °C in a 5% CO_2 atmosphere.

- Control: Untreated cells (no laser radiation, X-ray irradiation or Pt MN affection)
- N: Treated cells with Pt MN at a concentration of 100 μg mL^{-1}
- X6: Treated cells with X-ray irradiation at a radiation dose of 6 Gy after 4 h
- NX6: Treated cells firstly with Pt MN at a concentration of 100 μg mL^{-1} for 4 h followed by irradiation with X-ray at a radiation dose of 6 Gy
- L1.5: Treated cells with laser radiation at a power density of 1.5 W cm^{-2} for 10 min after 4 hx
- NL1.5: Treated cells firstly with Pt MN at a concentration of 100 μg mL^{-1} for 4 h followed by laser radiation at a power density of 1.5 W cm^{-2} for 10 min
- L1.5X6: Treated cells firstly with laser radiation at a power density of 1.5 W cm^{-2} for 10 min after 4 h, and then immediately irradiated with X-ray at a radiation dose of 6 Gy
- NL1.5X6: Treated cells firstly with Pt MN at a concentration of 100 μg mL^{-1} for 4 h, followed by laser radiation at a power density of 1.5 W cm^{-2} for 10 min, and then immediately irradiated with X-ray at a radiation dose of 6 Gy

The incubation time for different groups of the cells were continued for 72 h at 37 °C and 5% CO_2, and then the cell viabilities were measured by the MTT assay.

2.8. Intracellular ROS measurement induce by treatment in C540 (B16/F10) cells

Fluorescence intensity (FI) of dichlorofluorescein (DCF) was used for measuring intracellular ROS production. Different groups of C540 (B16/F10) cells including control, L1.5, X6, L1.5X6, N, NL1.5, NX6 and NL1.5X6 were treated according to Section 2.7. Then, 100 μL of a fresh DCHF-DA solution (50 μmol L^{-1}) was added to these treated cells, in time between laser radiation and X-ray irradiation. After laser radiation or X-ray irradiation, the treated cells were incubated for 30 min, following by washing three times with PBS to remove the extracellular DCF. After that, 100 μL of a lysis buffer (containing 150 mmol L^{-1} NaCl, 0.1% Triton X-100, 50 mmol L^{-1} Tris-HCl, pH = 8.0) was added to each well, and after 30 min, the intensity of fluorescence emission at 520 nm was measured upon excitation at 485 nm, using the microplate reader (Biotek, USA).

2.9. Pt MN uptake in the C540 (B16/F10) cells

C540 (B16/F10) cells (1.0×10^6) were incubated with Pt MN (100 μg mL^{-1}) at 37 °C in a 5% CO_2 for 24 h. Then, the cells were washed with PBS three times. The cells were lysed and digested with aqua regia (nitric acid/hydrochloric acid 3:1 V/V). Platinum content of the cells was measured by inductively coupled plasma optical emission spectrometry (ICP-OES) using a Varian 730-ES (USA) and divided by the cell number.

2.10. Statistical analysis

At least three parallel measurements were conducted for each

quantity. Multiple t-test, one way ANOVA with a Tukey posthoc was used to measure the statistical significance of the results using GraphPad (Prism 6) software. A p-value of less than 0.05 was considered statistically significant.

3. Results and discussion

Application of nanomaterials in medicine has different pros and cons, such as toxicity (or biocompatibility), stability and easy fabrication. Encountering metallic nanomaterials with electromagnetic waves induces a resonance between oscillation of the electrons and electromagnetic wave and produces a great energy absorption that is then dissipated to heat. This property of metal nanomaterials leads to their employment as efficient sensitizers of NIR light or X-ray in tumor therapy [45–47]. Pt nanomaterials are interested in nanomedicine due to high X-ray absorption ability arising from the high atomic number and X-ray attenuation coefficient (of 4.99 $cm^2 g^{-1}$ at 100 KeV) [48], compared to soft tissues and water in the biological media. This means that the Pt-contained tissues absorb more energy of X-rays, and their distortion needs lower radiation dose of X-ray. Pt nanomaterials also represent low toxicity making future inspiring applications. Up to now, limited researches have focused on application of Pt nanomaterials as sensitizers of light in cancer therapy [44,49].

Fig. 1 shows FESEM images of Pt MN recorded at various magnifications. The low-magnified images revealed that Pt MN comprised particles of various sizes. Higher magnified images revealed that each particle was sponge-resemble, and ensembles of very small adhered particles providing a highly porous structure. The pore size was estimated as < 11 nm from the highest-magnified image. Different magnified TEM images of Pt MN are also depicted in Fig. 2. These images confirm the information attained by FESEM, and better display the highly porous structure of Pt MN. Pt MN comprised adhered Pt dots of about 7 nm, forming about 5-nm pores.

As for inspection of the stability of the Pt MN suspension with a typical concentration of 500 μg mL^{-1} prepared in DI water, UV–vis spectra were recorded for the as-synthesized sample, and after centrifugation at 1000 rpm for 1, 2 and 5 min. The data is shown in Fig. 3. The spectra confirmed the 808-nm light absorbance ability of Pt MN, and its physical stability in DI water. For the long-term stability, we stored Pt MN suspensions with two concentrations of 0.1 and 1.0 mg mL^{-1} in DI water for several months. No visual sedimentation or agglomeration was observed at least for two months.

To assess toxicity, we measured PTT efficacy, X-PDT ability and PTT/X-PDT effect of Pt MN on the C540 (B16/F10) cells and cell viability. First of all, cytotoxicity of Pt MN was assessed by seeding the C540 (B16/F10) cells in the presence of different concentrations of Pt MN (with no any radiation) for 24 h, and the cell viability was quantified using the MTT assay. Cytotoxicity of Pt MN toward the cells in the presence of different concentrations of Pt MN after 72 h will be reported shortly (vide infra). Fig. 4 shows the treated cells' viability with Pt MN indicating a significant decrease ($p < 0.05$) in viability, compared to the control cells. The cell viability decreased upon increment in the Pt MN concentration in a dose-dependent manner. A Pt MN concentration of 10 μg mL^{-1} represented a viability of 97%, while 100 μg mL^{-1} of Pt MN induced a decreased viability of ~57%. Quantitative measurements of platinum content indicated an uptake level of 6 ng $cell^{-1}$ after 24 h. Although Pt NPs were reported to have low toxicity [50], the increased cytotoxicity of Pt MN in this study can be related to its mesoporous structure. Cytotoxicity of mesoporous ruthenium [51], carbon [52] and magnesia [53] has also been reported. In a study, toxicity of Pt nanodendrimer (PtNDs) toward Hela cells was attributed to Pt ions release from PtNDs [44]. Meantime, genotoxic stress [54], oxidizing of DNA [55] and reduction of the cell glutathione level [56] have also been suggested as other reasons for cytotoxicity of Pt nanomaterials.

To inspect the effect of 10 min laser radiation on the C540 (B16/F10) cells at two power densities of 1.0 and 1.5 W cm^{-2} (L1 and L1.5),

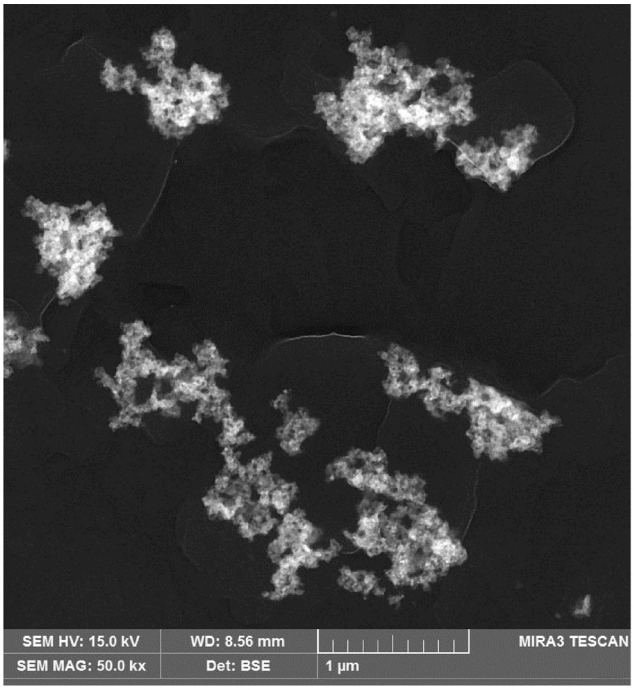

(A)

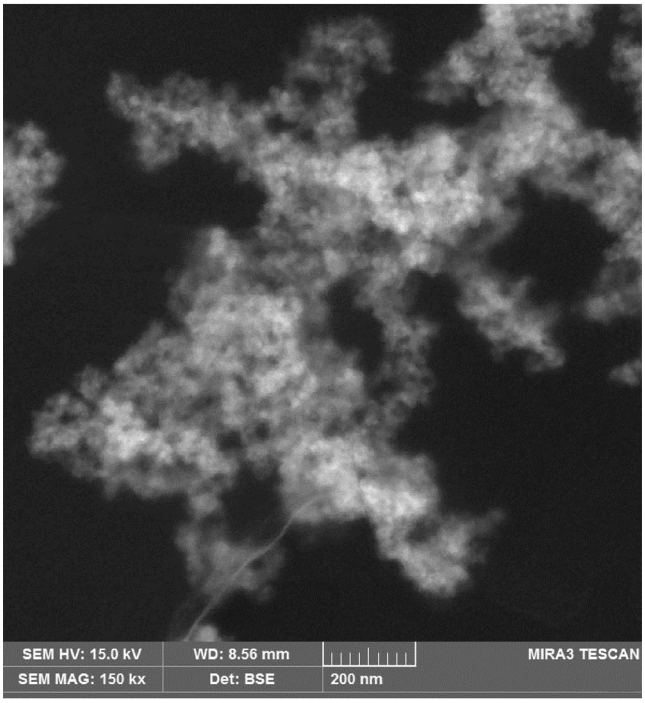

(B)

Fig. 1. FESEM images of Pt MN at two different magnifications.

the cell viability (with respect to the control cells) was evaluated by the MTT assay, and the obtained results are presented in Fig. 4. The results indicated decrement in the cell viability upon laser radiation at 1.0 and 1.5 W cm^{-2} to 96 and 80%, respectively. These results confirmed that the laser light was approximately compatible with the cells and did not induce significant damage to the cells. Statistical analysis showed no significant differences between the viability values of the cells irradiated at these two power densities of laser and the untreated ones ($p > 0.05$). Furthermore, PTT effect of Pt MN on C540 (B16/F10) cells was evaluated with laser radiation to the cells (1.0 and 1.5 W cm^{-2})

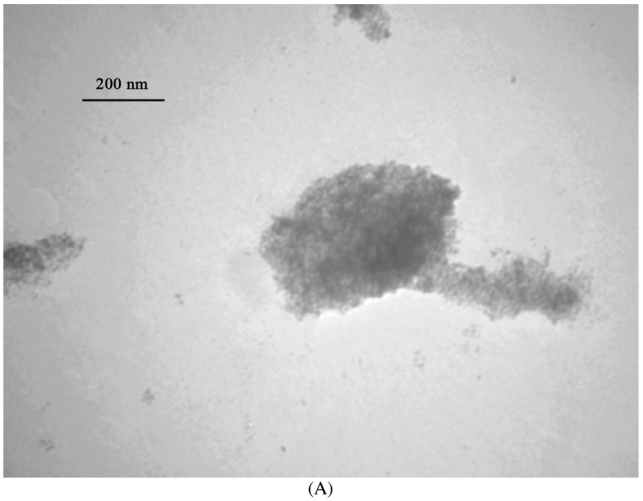

(A)

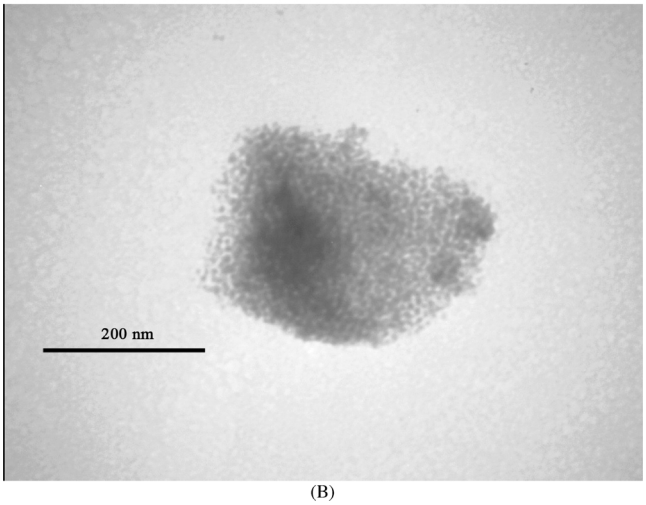

(B)

Fig. 2. TEM images of Pt MN at two different magnifications.

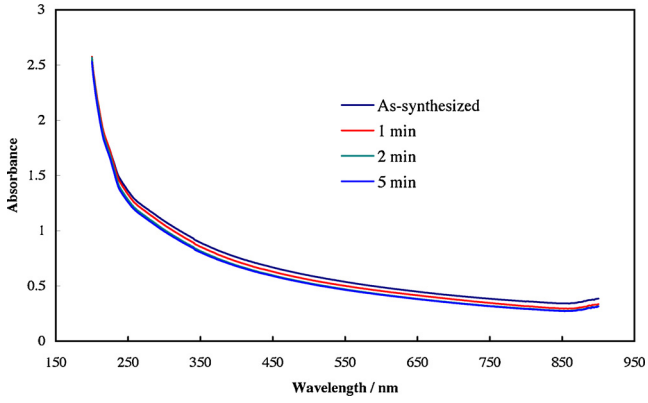

Fig. 3. UV–vis spectra recorded for the as-synthesized sample, and after centrifugation at 1000 rpm for 5 min.

after 4 h of incubation with different concentrations of Pt MN (10, 50 and 100 μg mL^{-1}). Fig. 4 shows the obtained results for NL1 and NL1.5 groups (at 100 μg mL^{-1} Pt MN), indicating cell viability decrement so that it reached 53 and 40% at 1.0 and 1.5 W cm^{-2}, respectively. Temperature increment of the C540 (B16/F10) cell medium in NL1 and NL1.5 groups was measured to be 6.0 ± 0.5 and 9.2 ± 0.8 °C upon laser radiation at power densities of 1.0 and 1.5 W cm^{-2}, respectively. Therefore, the capability of Pt MN as a photo-thermal transducer for C540 (B16/F10) cells is confirmed.

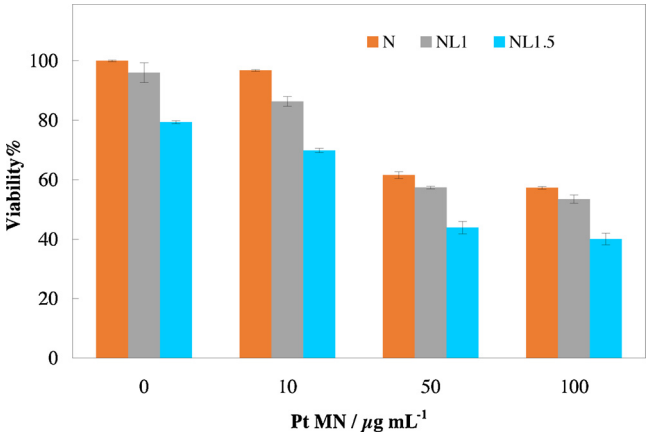

Fig. 4. Viability of C540 (B16/F10) cell after exposure to different concentrations of Pt MN after radiation for 10 min with 808-nm laser light at 1.0 and 1.5 W cm^{-2}, that was measured after 24 h incubation time. L0, L1.0 and L1.5 mean without laser radiation, radiation with laser at power density of 1.0 and radiation with laser at power density of 1.5 W cm^{-2}, respectively.

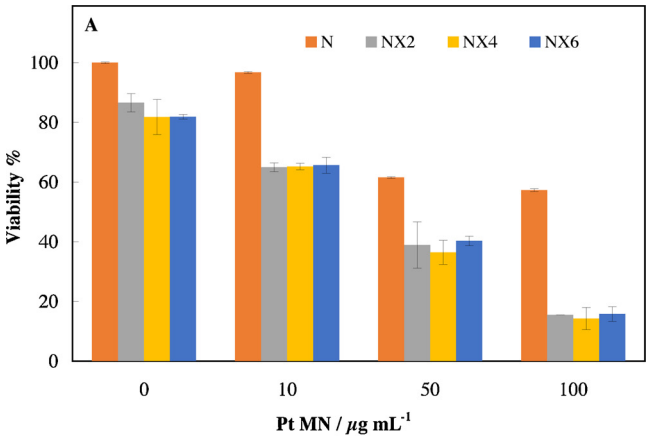

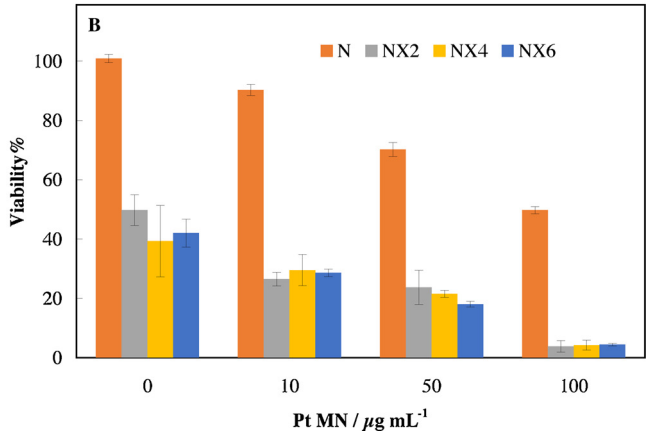

Fig. 5. Viability of C540 (B16/F10) cell after exposure to different concentrations of Pt MN after irradiation with X-ray at radiation doses of 2, 4 and 6 Gy, that was measured after 24 h (A) and 72 h (B) incubation time. × 0, X2.0, X4.0 and X6.0 mean without X-ray irradiation, irradiation at dose of 2 Gy, irradiation at dose of 4 Gy and irradiation at dose of 6 Gy, respectively.

Then, X-PDT effect of Pt MN on C540 (B16/F10) cells was evaluated by X-ray irradiation (at 2, 4 and 6 Gy) without or with different concentrations of Pt MN. Fig. 5A and B show the results of such treatment on the cell viability after 24 and 72 h, respectively. Cell viability assessment after 72 h was performed to inspect the long-term efficacy of

X-PDT. Without X-PDT, the cell viabilities upon treatment with different concentrations of Pt MN at two incubation times of 24 and 72 h (N) were nearly the same. It suggests dividing inhibition as well as proliferation of the cells by Pt MN during 72 h incubation. Without Pt MN affection, the cell viabilities upon treatment with different doses of RT of 2, 4 and 6 Gy (X2, X4 and X6) decreased to nearly the same value of 80% after 24 h. It seems that RT effect was insignificant during this time period. After 72 h, the cell viabilities upon treatment with different doses of RT of 2, 4 and 6 Gy (X2, X4 and X6, without Pt MN affection) reached about 50%. Therefore, RT needed a typical time period of 72 h to affect the cell viability. Upon both X-ray irradiation and Pt MN affection (NX2, NX4 and NX6), the cell viability significantly decreased. For example, the cell viability reached 15.8 and 4.0% after 24 h and 72 h, respectively, upon treatment with 100 μg mL^{-1} Pt MN along with X-PDT. The results demonstrated the effectiveness of Pt MN as a radiosensitizer for enhancing the RT efficacy. Moreover, RT treatment was not completed after 24 h, and decrement in the cell viability was deeper after 72 h, suggesting the effectiveness of X-PDT at longer times. However, at all of the Pt MN concentrations, statistical analysis of the cell viability values after 24 or 72 h showed no significant difference between all of the RT doses ($p > 0.05$). Therefore, it seems that 2 Gy was enough to activate all of the Pt MN concentrations. It should be noted that X-PDT induced no noticeable temperature increment of the C540 (B16/F10) cell medium.

To evaluate the combined effects of Pt MN, laser radiation and X-ray irradiation, we assessed the cell viability after 72 h for the N, X6, NX6, L1.5, NL1.5, L1.5X6 and NL1.5X6 ps, and the results are shown in Fig. 6. The cell viability values indicated that combination of laser radiation and X-PDT induced the highest activation of Pt MN, and a marked cell death. Statistical analysis of these results indicated that the entire cell viabilities reported in Fig. 6 had significant differences ($p < 0.05$). Therefore, there was an order of treatment efficacy between the groups as L1.5 < N < X6 < NL1.5 < L1.5X6 < NX6 < NL1.5X6, with significant differences ($p < 0.05$).

Domination of synergistic effect in NL1.5X6 was explored by calculation of the projected additive value [57]. This value was estimated by multiplying the cell viabilities of NL1.5 and NX6 groups to be 1.6%. Considering the viabilities of NL1.5X6 (1.2%), NL1.5 (40.1%) and NX6 (4.1%) groups, it was witnessed that the NL1.5X6 viability value was lower than projected additive value. Therefore, a synergistic effect dominated for the effects of Pt MN, laser radiation and X-ray irradiation.

For inspection of the probable mechanism of cell killing upon PTT, X-PDT or PTT/X-PDT, intracellular ROS was evaluated after treatment by measuring FI of DCF. DCFH-DA passively enters the cells, and is deacetylated by esterases to the non-fluorescent DCFH. DCFH interacts

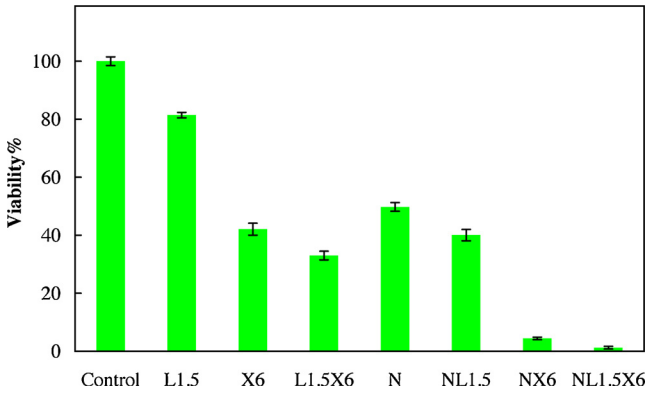

Fig. 6. Viability of C540 (B16/F10) cell after exposure to Pt MN (100 μg mL^{-1}) and radiation with laser and/or irradiation with X-ray. L1.5 means laser irradiation at power density of 1.5 W cm^{-2}, X6 means X-ray irradiation at dose of 6 Gy, N means with pt MN affection.

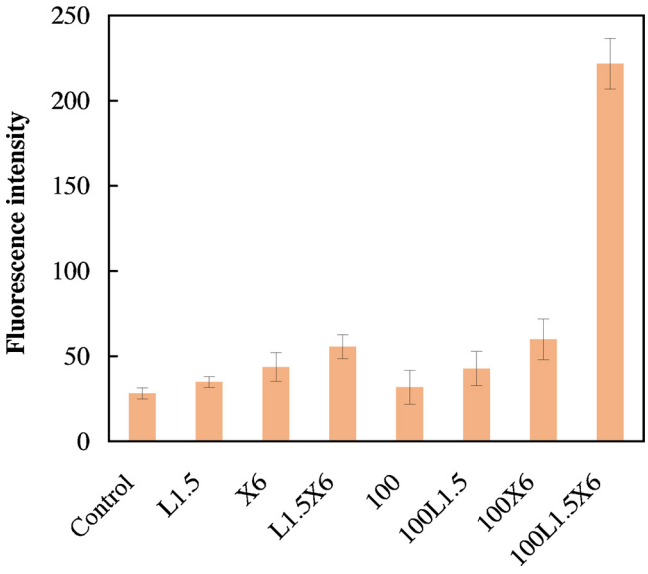

Fig. 7. FI of DCF in C540 (B16/F10) cell after exposure to Pt MN (100 μg mL^{-1}) and radiation with laser and/or irradiation with X-ray. L1.5 means laser irradiation at power density of 1.5 W cm^{-2}, X6 means X-ray irradiation at dose of 6 Gy, N means with pt MN affection.

with ROS, and is converted to fluorescent DCF with an emission light at 520 nm. Fig. 7 shows FI for different groups. FI of control cells was considered as a base signal. Based on the results, treated cells in L1.5 and N groups showed no significant difference in their FIs (and intracellular ROS levels), compared to control. Therefore, radiation of laser or treatment with Pt MN of the cells alone did not intensify ROS generation within the cells; any cell killing effect observed for L1.5 group was due to the temperature increment. On the other hand, FI of X6, NL1.5, NX6 and L1.5X6 groups increased slightly. Hence, the killing effect observed for these groups was due to a bit ROS generation. These results indicated that efficacy of cell killing in the groups X6 and NX6 were just due to ROS generation and laser radiation into Pt MN also generated ROS (NL1.5 group). While, FI of NL1.5X6 was the highest with a high significant difference with the other groups. Therefore, PTT/X-PDT induced the highest ROS production that induced higher destroying grade in the cancer cells. Ultimately, both heat generation and ROS production induce cell killing with a majority effect arose from the later.

In the literature, there are few reports on the application of platinum nanostructures as a laser light and X-ray transducer, and also combined effects of laser radiation and X-ray irradiation using a sensitizer. Radiosensitization effect of PtNDs on Hela cells under 6 MV photon beams was reported [44]. PtNDs irradiation led to enhanced apoptotic cell death. The viability of 4T1 cells that firstly treated with Au@Pt nanodendrimer (NDs, 50 μg mL^{-1}), then exposed to laser radiation (808 nm, 1 W cm^{-2}, 10 min), and finally irradiated by X-ray (4 Gy) decreased to 30%, which was 42% lower than the viability upon Au@Pt NDs/PTT treatment, and 25% lower than the viability attained from Au@Pt NDs/RT treatment [58]. Li et al. applied polyethylene glycol and folic acid-modified PtCu octopod nanoframes as a strong absorbing agent of NIR light and X-ray to destroy HepG2 cells [59]. The results showed that combined PTT (808 nm, 2.4 W cm^{-2}, 5 min) and X-PDT (120 kVp, 10 Gy, 10 min) treatment decreased the viability below 5% that was about 40% lower than that of X-PDT alone and 20% lower than that of PTT alone. Damage to DNA strands and apoptosis occurred during the dual treatments. Bi-based sensitizers were also utilized for combined NIR light and X-ray energy conversion. BEL-7402 cancer cells were treated with bovine serum albumin-coated BiOI@Bi_2S_3 nanoparticles (100 μg mL^{-1}), NIR light radiation (at 1 W cm^{-2}, 10 min) and X-ray irradiation (at 8 Gy, 10 min) [60]. This treatment led to a 2.1%

cell survival and high levels of ROS production, a deeper effect that was attained compared to single treatment. Ma et al. also introduced polyvinylpyrrolidone coated porous Bi nanospheres as a radiosensitizer to trigger X-ray deposition as well as in PTT as a photoabsorbing agent to destroy Hela cell [48]. As for a metal-free sensitizer, polyglutamic acid nanogels loaded with polypyrrole were developed for PTT/X-PDT to enhance the efficacy of cancer cell treatment [41]. Compared to a single PTT or X-PDT, dual treatment showed better treatment outcomes at the same concentration of the sensitizer.

Interaction of photon radiation occurs with the sensitizer electrons leading to energy loss through ionization, or with the sensitizer nuclei resulting in bremsstrahlung radiation. In the relatively low kV energy range, where the photoelectric effect is predominant, atomic number of the sensitizer and radiation energy determine the ratio of these processes [61], wherein photon absorption depends on the term $(Z/E)^3$, where Z is the atomic number and E is the photon energy (in KV energy range) [46]. For this reason, high-Z nanosensitizers can provide significantly higher cross sections for photon absorption in the low-to-medium kV energy range, compared to soft tissues and water. Therefore, transition metal nanostructure-based sensitizers are ideal for radiation treatment. X-PDT with metal nanostructures induces a great number of photoelectrons and Auger electrons, which induce matter ionization, ROS generation, DNA damage, and cell apoptosis and necrosis [32]. Using the MeV energy range or heavy charged particles and enhanced radiosensization of metal nanomaterials increase biological mechanisms such as oxidative stress, cell cycle disruption and DNA repair inhibition [44]. Porcel et al. showed an increase in the DNA double-to-single strands break ratio in plasmid DNA when using Pt NPs with ion radiation [62]. An increased amount of strand break was also observed by Xiao et al. who irradiated AuNPs by electrons [63]. Sech et al. and Kobayashi et al. found out that Pt or its derivatives could increase DSB in DNA under X-ray exposure [64,65]. Interaction of X-ray with Pt led to radical generation that mediated the breaks in the DNA strand [66].

Collective excitation of free electrons in noble metals such as Pt can be performed by light in resonance with an electromagnetic field [67]. Because nanomaterials have enhanced near-surface electric fields (localized surface plasmon resonances), they show an intense light absorption [68,69]. Upon exposure to NIR light, the absorbed light is converted to heat, leading to motivation of hyperthermia, damage, necrosis and osteolysis in the cancer cells [68–71]. On the other hand, laser radiation can improve oxygen status in tumor cells and improve the efficacy of X-PDT [36]. Our results showed that Pt MN could be applied as a nanoscale heat source for cancer therapy, and provide a completely new route for practical applications.

4. Conclusion

In summary, we have synthesized Pt MN as a novel NIR photosensitizer for PTT and X-ray absorbing agent for X-PDT of melanoma cancer cells. Pt MN effectively killed cancer C540 (B16/F10) cells under PTT, X-PDT and PTT/X-PDT. PTT/X-PDT was performed with the most effectiveness and synergistic effect as compared to PTT or X-PDT alone. ROS production was the reason for treatment effect of PTT/X-PDT, while heat increased during PTT. The results give a new route to construct a noble metallic agent as an efficient photo/radio sensitizer that integrates the two (or maybe more) therapeutic modalities for cancer treatment with a superior therapeutic outcome. The porosity, size and plasmonic properties of PT MN also make it a promising candidate for drug loading with promising clinical potentials for efficient cancer therapy.

Acknowledgments

The paper has been extracted from F. Salehi's thesis supported by the Research Council of Shiraz University of Medical Sciences (18806).

References

[1] R.L. Siegel, K.D. Miller, S.A. Fedewa, D.J. Ahnen, R.G.S. Meester, A. Barzi, A. Jemal, Colorectal cancer statistics, CA: Cancer J. Clinicians 67 (2017) 177–193.
[2] Z. Yazdani, H. Yadegari, H. Heli, A molecularly imprinted electrochemical nanobiosensor for prostate specific antigen determination, Anal. Biochem. 566 (2019) 116–125.
[3] R. Nazari-Vanani, K. Karimian, N. Azarpira, H. Heli, Capecitabine-loaded nanoniosomes and evaluation of anticancer efficacy, Artif. Cells Nanomed. Biotechnol. 47 (2019) 420–426.
[4] M. Noorani, N. Azarpira, K. Karimian, H. Heli, Erlotinib-loaded albumin nanoparticles: a novel injectable form of erlotinib and its in vivo efficacy against pancreatic adenocarcinoma ASPC-1 and PANC-1 cell lines, Int. J. Pharm. 531 (2017) 299–305.
[5] S. Akhtartavan, M. Karimi, K. Karimian, N. Azarpira, M. Khatami, H. Heli, Evaluation of a self-nanoemulsifying docetaxel delivery system, Biomed. Pharmacother. 109 (2019) 2427–2433.
[6] L. Cheng, C. Wang, L.Z. Feng, K. Yang, Z. Liu, Functional nanomaterials for phototherapies of cancer, Chem. Rev. 114 (2014) 10869–10939.
[7] X. Zhen, C. Xie, K.Y. Pu, Temperature-correlated afterglow of a semiconducting polymer nanococktail for imaging-guided photothermal therapy, Angew. Chemie Int. Ed. 57 (2018) 3938–3942.
[8] S.S. Lucky, K.C. Soo, Y. Zhang, Nanoparticles in photodynamic therapy, Chem. Rev. 115 (2015) 1990–2042.
[9] X.D. Ren, X.Y. Hao, H.C. Li, M.R. Ke, B.Y. Zheng, J.D. Huang, Progress in the development of nanosensitizers for x-ray-induced photodynamic therapy, Drug Discov. Today 23 (2018) 1791–1800.
[10] J.J. Zhang, X. Zhen, P.K. Upputuri, M. Pramanik, P. Chen, K.Y. Pu, Activatable photoacoustic nanoprobes for in vivo ratiometric imaging of peroxynitrite, Adv. Mater. 29 (2017) 1604764.
[11] N. Sattarahmady, N. Azarpira, A. Hosseinpour, H. Heli, T. Zare, Albumin coated arginine-capped magnetite nanoparticles as a paclitaxel vehicle: physicochemical characterizations and in vitro evaluation, J. Drug Deliv. Sci. Technol. 36 (2016) 68–74.
[12] H. Xing, X. Zheng, Q. Ren, W. Bu, W. Ge, Q. Xiao, S. Zhang, C. Wei, H. Qu, Z. Wang, Y. Hua, L. Zhou, W. Peng, K. Zhao, J. Shib, Computed tomography imaging-guided radiotherapy by targeting upconversion nanocubes with significant imaging and radiosensitization enhancements, Sci. Rep. 3 (2013) 1751.
[13] J. Zheng, G. Perkins, A. Kirilova, C. Allen, D.A. Jaffray, Multimodal contrast agent for combined computed tomography and magnetic resonance imaging applications, Invest. Radiol. 41 (2006) 339–348.
[14] X. Jiang, S. Zhang, F. Ren, L. Chen, J.F. Zeng, M. Zhu, Z.X. Cheng, M.Y. Gao, Z. Li, Ultrasmall magnetic cufese2 ternary nanocrystals for multimodal imaging guided photothermal therapy of cancer, ACS Nano 11 (2017) 5633–5645.
[15] Y.Y. Cui, J. Yang, Q.F. Zhou, P. Liang, Y.L. Wang, X.Y. Gao, Y.T. Wang, Renal clearable Ag nanodots for in vivo computer tomography imaging and photothermal therapy, ACS Appl. Mater. Interfaces 9 (2017) 5900–5906.
[16] H.-F. Cui, Y.-F. Bai, W.-W. Wu, X. He, J.H. Luong, Modification with mesoporous platinum and poly(pyrrole-3-carboxylic acid)-based copolymer on boron-doped diamond for nonenzymatic sensing of hydrogen peroxide, J. Electroanal. Chem. 766 (2016) 52–59.
[17] H. Fan, Z. Guo, L. Gao, Y. Zhang, D. Fan, G. Ji, B. Du, Q. Wei, Ultrasensitive electrochemical immunosensor for carbohydrate antigen 72-4 based on dual signal amplification strategy of nanoporous gold and polyaniline–Au asymmetric multicomponent nanoparticles, Biosens. Bioelectron. 64 (2015) 51–56.
[18] G.H. Wang, Z. Cao, D. Gu, N. Pfander, A.C. Swertz, B. Spliethoff, H.J. Bongard, C. Weidenthaler, W. Schmidt, R. Rinaldi, Nitrogen-doped ordered mesoporous carbon supported bimetallic ptco nanoparticles for upgrading of biophenolics, Angew. Chemie Int. Ed. 55 (2016) 8850–8855.
[19] A. Rahi, K. Karimian, H. Heli, Nanostructured materials in electroanalysis of pharmaceuticals, Anal. Biochem. 497 (2016) 39–47.
[20] H. Heli, A. Rahi, Synthesis and applications of nanoflowers, Recent Pat. Nanotechnol. 10 (2016) 86–115.
[21] M. Negahdary, A. Moradi, H. Heli, Application of electrochemical aptasensors in detection of cancer biomarkers, Biomed. Res. Ther. 6 (2019) 3315–3324.
[22] H. Heli, F. Pourbahman, N. Sattarahmady, Nanoporous nickel microspheres: synthesis and application for the electrocatalytic oxidation and determination of acyclovir, Anal. Sci. 28 (2012) 503–510.
[23] Q. Pu, J. Li, J. Qiu, X. Yang, Y. Li, D. Yin, X. Zhang, Y. Tao, S. Sheng, G. Xie, Universal ratiometric electrochemical biosensing platform based on mesoporous platinum nanocomposite and nicking endonuclease assisted DNA walking strategy, Biosens. Bioelectron. 94 (2017) 719–727.
[24] Z. Cui, D. Wu, Y. Zhang, H. Ma, H. Li, B. Du, Q. Wei, H. Ju, Ultrasensitive electrochemical immunosensors for multiplexed determination using mesoporous platinum nanoparticles as nonenzymatic labels, Anal. Chim. Acta 807 (2014) 44–50.
[25] L. Wang, Y. Yusuke, Synthesis of mesoporous Pt nanoparticles with uniform particle size from aqueous surfactant solutions toward highly active electrocatalysts, Chem. Eur. J. 17 (2011) 8810–8815.
[26] D. Schaue, W.H. McBride, Opportunities and challenges of radiotherapy for treating cancer, Nat. Rev. Clin. Oncol. 12 (2015) 527–540.
[27] J.F. Hainfeld, L. Lin, D.N. Slatkin, F.A. Dilmanian, T.M. Vadas, H.M. Smilowitz, Gold nanoparticle hyperthermia reduces radiotherapy dose, Nanomedicine 10 (2014) 1609–1617.
[29] W.P. Fan, W.B. Bu, Z. Zhang, B. Shen, H. Zhang, Q.J. He, D.L. Ni, Z.W. Cui, K.L. Zhao, J.W. Bu, J.L. Du, J.N. Liu, J.L. Shi, X-ray radiation-controlled no-release

for on-demand depth-independent hypoxic radiosensitization, Angew. Chemie Int. Ed. 54 (2015) 14026–14030.
[30] H. Harada, M. Hiraoka, Hypoxia-inducible factor 1 in tumor radioresistance, Curr. Signal Transduct. Ther. 5 (2010) 188–196.
[31] J. Li, W.T. Shang, Y. Li, S.R. Fu, J. Tian, L.G. Lu, Advanced nanomaterials targeting hypoxia to enhance radiotherapy, Int. J. Nanomedicine 13 (2018) 5925–5936.
[32] K. Haume, S. Rosa, S. Grellet, M.A. Smialek, K.T. Butterworth, A.V. Solov'yov, K.M. Prise, J. Golding, N.J. Mason, Gold nanoparticles for cancer radiotherapy: a review, Cancer Nanotechnol. 7 (2016) 8.
[33] S.H. Cho, Estimation of tumour dose enhancement due to gold nanoparticles during typical radiation treatments: a preliminary Monte Carlo study, Phys. Med. Biol. 50 (2005) 163–173.
[34] R. Brown, M. Tehei, S. Oktaria, A. Briggs, C. Stewart, K. Konstantinov, A. Rosenfeld, S. Corde, M. Lerch, High-Z nanostructured ceramics in radiotherapy: first evidence of Ta2O5-induced dose enhancement on radioresistant cancer cells in an mV photon field, Part. Part. Syst. Charact. 31 (2014) 500–505.
[35] S. Her, D.A. Jaffray, C. Allen, Gold nanoparticles for applications in cancer radiotherapy: mechanisms and recent advancements, Adv. Drug Deliv. Rev. 109 (2017) 84–101.
[36] G.S. Song, C.H. Ji, C. Liang, X.J. Song, X. Yi, Z.L. Dong, K. Yang, Z. Liu, TaOx decorated perfluorocarbon nanodroplets as oxygen reservoirs to overcome tumor hypoxia and enhance cancer radiotherapy, Biomaterials 112 (2017) 257–263.
[37] S.H. Cho, Estimation of tumour dose enhancement due to gold nanoparticles during typical radiation treatments: a preliminary Monte Carlo study, Phys. Med. Biol. 50 (2005) 163–173.
[38] W.Z. Xie, W. Friedland, W.B. Li, C.Y. Li, U. Oeh, R. Qiu, J.L. Li, C. Hoeschen, Simulation on the molecular radiosensitization effect of gold nanoparticles in cells irradiated by x-rays, Phys. Med. Biol. 60 (2015) 6195–6212.
[39] L. Sellami, S. Lacombe, D. Hunting, R.J. Wagner, M.A. Huels, Novel apparatus to measure hyperthermal heavy ion damage to DNA: strand breaks, base loss, and fragmentation, Rev. Sci. Instrum. 78 (2007) 085111.
[40] E. Porcel, S. Liehn, H. Remita, N. Usami, K. Kobayashi, Y. Furusawa, C. Le Sech, S. Lacombe, Platinum nanoparticles: a promising material for future cancer therapy? Nanotechnology 21 (2010) 085103.
[41] Y.W. Zhou, Y. Hu, W.J. Sun, S.Y. Lu, C. Cai, C. Peng, J. Yu, R. Popovtzer, M.W. Shen, X.Y. Shi, Radiotherapy-sensitized tumor photothermal ablation using γ-Polyglutamic acid nanogels loaded with polypyrrole, Biomacromolecules 19 (2018) 2034–2042.
[42] G.S. Song, C. Liang, X. Yi, Q. Zhao, L. Cheng, K. Yang, Z.A. Liu, Perfluorocarbon-loaded hollow Bi2Se3 nanoparticles for timely supply of oxygen under near-infrared light to enhance the radiotherapy of cancer, Adv. Mater. 28 (2016) 2716–2723.
[43] N.N. Ma, Y.W. Jiang, X.D. Zhang, H. Wu, J.N. Myers, P.D. Liu, H.Z. Jin, N. Gu, N. He, F.G. Wu, Z. Chen, Enhanced radiosensitization of gold nanospikes via hyperthermia in combined cancer radiation and photothermal therapy, ACS Appl. Mater. Interfaces 8 (2016) 28480–28494.
[44] K.A.M. Afiq, R. Ab Rashid, R.M. Lazim, N. Dollah, K.A. Razak, W.N. Rahman, Evaluation of radiosensitization effects by platinum nanodendrites for 6-MV photon beam radiotherapy, Radiat. Phys. Chem. 150 (2018) 40–45.
[45] G. Baffou, R. Quidant, C. Girard, Heat generation in plasmonic nanostructures: influence of morphology, Appl. Phys. Lett. 94 (2009) 153109.
[46] A. Samadi, H. Klingberg, L. Jauffred, A. Kjaer, P.M. Bendix, L.B. Oddershede, Platinum nanoparticles: a non-toxic, effective and thermally stable alternative plasmonic material for cancer therapy and bioengineering, Nanoscale 10 (2018) 9097–9107.
[47] P. Wang, H. Tang, P. Zhang, Plasmonic nanoparticle-based hybrid photosensitizers with broadened excitation profile for photodynamic therapy of cancer cells, Sci. Rep. 6 (2016) 34981.
[48] G.C. Ma, X.J. Liu, G.Y. Deng, H.K. Yuan, Q.G. Wang, J. Lu, A novel theranostic agent based on porous bismuth nanosphere for CT imaging-guided combined chemo-photothermal therapy and radiotherapy, J. Mater. Chem. B 6 (2018) 6788–6795.
[49] Q.X. Ma, L. Cheng, F. Gong, Z.L. Dong, C. Liang, M.Y. Wang, L.Z. Feng, Y.G. Li, Z. Liu, C. Li, L. He, Platinum nanoworms for imaging-guided combined cancer therapy in the second near-infrared window, J. Mater. Chem. B 6 (2018) 5069–5079.
[50] H. Gehrke, J. Pelka, C.G. Hartinger, H. Blank, F. Bleimund, R. Schneider, D. Gerthsen, S. Brase, M. Crone, M. Turk, D. Marko, Platinum nanoparticles and their cellular uptake and DNA platination at non-cytotoxic concentrations, Arch. Toxicol. 85 (2011) 799–812.
[51] S. Ramasamy, D. Bennet, S. Kim, Synthesis of hollow mesoporous ruthenium nanoparticles: evaluation of physico-chemical properties and toxicity, RSC Adv. 5 (2015) 79616–79623.
[52] Y.N. Chen, Y. Yang, B.L. Xu, S.H. Wang, B. Li, J. Ma, J. Gao, Y.Y. Zuo, S.J. Liu, Mesoporous carbon nanomaterials induced pulmonary surfactant inhibition, cytotoxicity, inflammation and lung fibrosis, J. Environ. Sci. 62 (2017) 100–114.
[53] M.S. Hamdy, N.S. Awwad, A.M. Alshahrani, Mesoporous magnesia: synthesis, characterization, adsorption behavior and cytotoxic activity, Mater. Des. 110 (2016) 503–509.
[54] P.V. Asharani, N. Xinyi, M.P. Hande, S. Valiyaveettil, DNA damage and p53-mediated growth arrest in human cells treated with platinum nanoparticles, Nanomedicine 5 (2010) 51–64.
[55] M. Kutwin, E. Sawosz, S. Jaworski, M. Wierzbicki, B. Strojny, M. Grodzik, A. Chwalibog, Assessment of the proliferation status of glioblastoma cell and tumour tissue after nanoplatinum treatment, PLoS One 12 (2017) e0178277.
[56] J. Pelka, H. Gehrke, M. Esselen, M. Turk, M. Crone, S. Brase, T. Muller, H. Blank, W. Send, V. Zibat, P. Brenner, R. Schneider, D. Gerthsen, D. Marko, Cellular uptake of platinum nanoparticles in human colon carcinoma cells and their impact on cellular redox systems and DNA integrity, Chem. Res. Toxicol. 22 (2009) 649–659.
[57] Q. Xiao, X. Zheng, W. Bu, W. Ge, S. Zhang, F. Chen, H. Xing, Q. Ren, W. Fan, K. Zhao, Y. Hua, J. Shi, A Core/Satellite multifunctional nanotheranostic for in vivo imaging and tumor eradication by Radiation/Photothermal synergistic therapy, J. Am. Chem. Soc. 135 (2013) 13041–13048.
[58] X. Liu, X. Zhang, M. Zhu, G. Lin, J. Liu, Z. Zhou, X. Tian, Y. Pan, PEGylated Au@Pt nanodendrites as novel theranostic agents for CT imaging and photothermal/radiation synergistic therapy, ACS Appl. Mater. Interfaces 9 (2017) 279–285.
[59] J.H. Li, X.Y. Zu, G.F. Liang, K.K. Zhang, Y.L. Liu, K. Li, Z. Luo, K.Y. Cai, Octopod PtCu nanoframe for dual-modal imaging-guided synergistic photothermal radiotherapy, Theranostics 8 (2018) 1042–1058.
[60] Z. Guo, S. Zhu, Y. Yong, X. Zhang, X. Dong, J. Du, J. Xie, Q. Wang, Z. Gu, Y. Zhao, Synthesis of BSA-coated BiOI@Bi2S3 semiconductor heterojunction nanoparticles and their applications for radio/photodynamic/photothermal synergistic therapy of tumor, Adv. Mater. 29 (2017) 1704136.
[61] F.M. Khan, J.P. Gibbons, Khan's the Physics of Radiation Therapy, Lippincott, Williams & Wilkins, 2014.
[62] E. Porcel, S. Liehn, H. Remita, N. Usami, K. Kobayashi, Y. Furusawa, C. Le Sech, S. Lacombe, Platinum nanoparticles: a promising material for future cancer therapy? Nanotechnology 21 (2010) 085103.
[63] F.X. Xiao, Y. Zheng, P. Cloutier, Y.H. He, D. Hunting, L. Sanche, On the role of low-energy electrons in the radiosensitization of DNA by gold nanoparticles, Nanotechnology 22 (2011) 465101.
[64] C.L. Sech, K. Takakura, C. Saint-Marc, H. Frohlich, M. Charlier, N. Usami, K. Kobayashi, Strand break induction by photoabsorption in DNA-bound molecules, Radiat. Res. 53 (2000) 454–458.
[65] K. Kobayashi, H. Frohlich, N. Usami, K. Takakura, C. Le Sec, Enhancement of X-ray-induced breaks in DNA bound to molecules containing platinum: a possible application to hadrontherapy, Radiat. Res. 157 (2002) 32–37.
[66] S.L. Liu, J.M. Piao, Y.C. Liu, J.L. Tang, P. Liu, D.P. Yang, L. Zhang, N. Ge, Z.Z. Jin, Q.X. Jiang, L.H. Cui, Radiosensitizing effects of different size bovine serum albumin-templated gold nanoparticles on H22 hepatoma-bearing mice, Nanomedicine 13 (2018) 1371–1383.
[67] P.K. Jain, X. Huang, I.H. El-Sayed, M.A. El-Sayad, Review of some interesting surface plasmon resonance-enhanced properties of noble metal nanoparticles and their applications to biosystems, Plasmonics 2 (2007) 107–118.
[68] P.K. Jain, X. Huang, I.H. El-Sayed, M.A. El-Sayed, Noble metals on the nanoscale: optical and photothermal properties and some applications in imaging, sensing, biology, and medicine, Acc. Chem. Res. 41 (2008) 1578–1586.
[69] E.S. Day, J.G. Morton, J.L. West, Nanoparticles for thermal cancer therapy, J. Biomech. Eng. 131 (2009) 74001.
[70] C. Wang, X. Cai, J. Zhang, X. Wang, Y. Wang, H. Ge, W. Yan, Q. Huang, J. Xiao, Q. Zhang, Y. Cheng, Trifolium-like platinum nanoparticle-mediated photothermal therapy inhibits tumor growth and osteolysis in a bone metastasis model, Small 11 (2015) 2080–2086.
[71] F. Rahimi-Moghaddam, N. Azarpira, N. Sattarahmady, Evaluation of a nanocomposite of PEG-curcumin-gold nanoparticles as a near-infrared photothermal agent: an in vitro and animal model investigation, Lasers Med. Sci. 33 (2018) 1769–1779.